INFLUENCE OF SPECIMEN DESIGN ON THE DEFORMATION AND FAILURE OF ZIRCALOY CLADDING

Douglas W. Bates[*], Donald A. Koss, and Arthur T. Motta
The Pennsylvania State University, University Park, PA 16802
douglas_w_bates@hotmail.com   koss@ems.psu.edu   atm2@psu.edu

Saurin Majumdar
Argonne National Laboratory, Argonne, IL 60439
majumdar@anl.gov

ABSTRACT

Experimental as well as computational analyses have been used to examine the deformation and failure behavior of ring-stretch specimens of Zircaloy-4 cladding tubes. The results show that, at least for plastically anisotropic unirradiated cladding, specimens with a small gauge length l to width w ratio ($l/w \approx 1$) exhibit pronounced non-uniform deformation along their length. As a result, specimen necking occurs upon yielding when the specimen is fully plastic. Finite element analysis indicates a minimum l/w of 4 before a significant fraction of the gauge length deforms homogeneously. A brief examination of the contrasting deformation and failure behavior between uniaxial and plane-strain ring tension tests further supports the use of the latter geometry for determining cladding failure ductility data that are relevant to certain reactivity-initiated accident conditions.

INTRODUCTION

In a reactivity-initiated accident (RIA), a control rod ejection or drop causes a sudden increase in reactor power, which in turn deposits a large amount of energy into the fuel[1]. The resulting thermal expansion of the fuel and fission gas release loads the cladding into the plastic regime and may cause it to fail. Currently, there is no consensus as to the exact nature of the loading on the cladding during an RIA. If failure is caused primarily by thermally-induced loading (i.e., deformation-controlled), cladding ductility controls failure. On the other hand, if loading is primarily due to gas pressure pulse (i.e., load-controlled), the ultimate tensile strength controls failure. In order to predict cladding survivability, there has been considerable interest and effort in supplementing integral RIA tests with separate-effects ring tests of cladding tubes. Such tests can give us insight into failure mechanisms and measure relevant mechanical properties (such as yield strength, ultimate tensile strength, uniform elongation, uniaxial stress-strain curve, etc.), for use in computer codes that attempt to predict cladding response during an RIA. The accuracy of such model predictions obviously depends on appropriate and accurate deformation and failure data. This study concerns itself with the proper development of ring tensile tests that (i) are similar to the loading conditions present in an RIA, (ii) measure the relevant mechanical properties and (iii) provide insight regarding the influence of the strain paths on the failure mechanisms present if Zircaloy cladding. Based on both experiments and computational modeling, we investigate the failure of Zircaloy tubing as a function of specimen geometry, and discuss the limitations of certain ring-test geometries in yielding failure ductility data that are applicable to RIA situations.

* # Currently U.S. Navy, Newport Beach, VA

DISCLAIMER

DISCLAIMER

**Portions of this document may be illegible
in electronic image products. Images are
produced from the best available original
document.**

EXPERIMENTAL PROCEDURE

For this study, several identical Zircaloy-4 cladding tubes were obtained from Sandvik Metals in the cold-worked, stress-relieved condition (CWSR). The tubes had an outer diameter of approximately 9.5 mm and a wall thickness of about 0.56 mm. The examination of the grain structure performed using light microscopy of etched specimens revealed elongated grains with an approximately 10:1 aspect ratio parallel to the tube axis. The elongated grains were approximately 10-15 μm long and 1-2 μm thick.

The present cladding tube material has the usual rolling or extruding texture, i.e., the basal planes tend to align with their basal poles inclined approximately $\pm$ 40° to the normal of the tube surface and oriented towards the tangential direction. The prism poles show a strong tendency to align along the tube axis, which is also consistent with previous observations for such cladding. These results show that the texture in this cladding results in basal and prism pole intensities as much as ten times their random value. As such, the Zircaloy-4 cladding studied here exhibits a crystallographic texture typical of the cold worked and stress relieved (CWSR) condition[2].

For in-service cladding failure of Zircaloy in which the cladding fails due to an axial split, the major strain direction is the hoop direction of the cladding tube, which is transverse to the cladding axis. Thus, *transverse* ring-stretch tests were performed on the cladding material as a means of determining its deformation and failure response. Three ring-stretch specimen geometries, shown in Figure 1, were utilized in this study. For uniaxial tension testing, two specimen geometries, designated type "C" and type "D", were examined. The type "C" specimen had a gauge length to width ratio of 1:1, while type "D" had the more conventional 4:1 gauge length to width ratio. In addition, a transverse plane-strain geometry, described previously[3], was also examined in this study. As shown in Figure 1c, such a geometry uses the constraints imposed by the notches to force the center section into a near plane-strain deformation state.
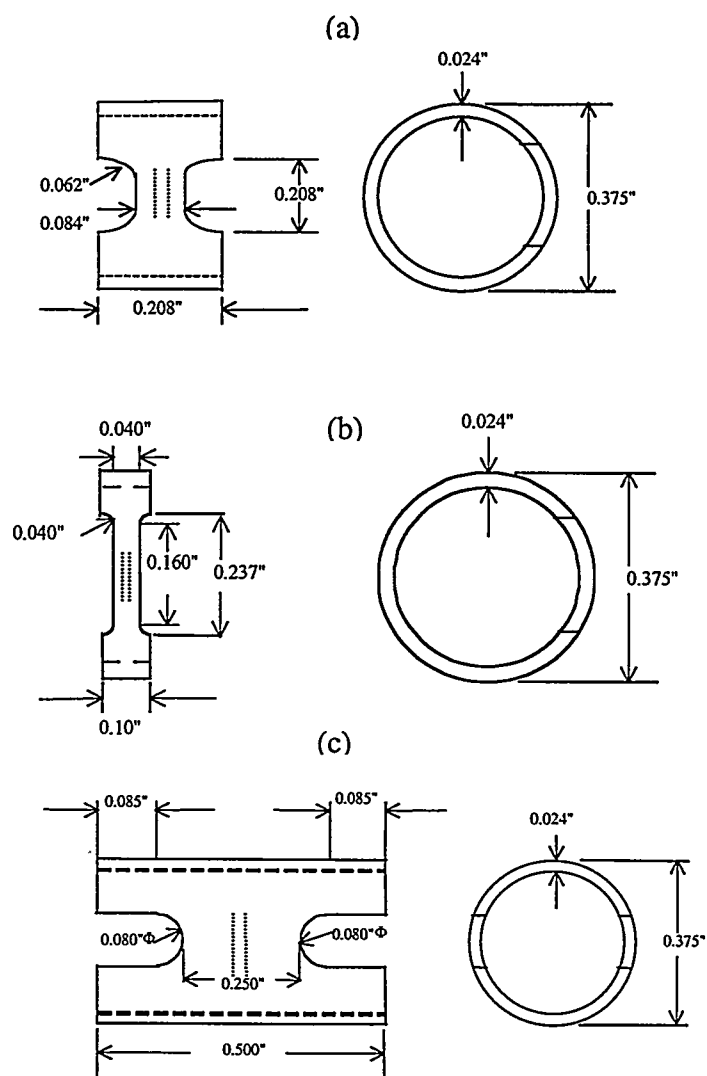
Figure 1 : Specimen Dimensions for mechanical testing. (a) type "C" specimen; (b) type "D" specimen and (c) plane strain specimen.

Local strains as well as strain distributions along the specimen length were experimentally determined using the microhardness indentation gridding procedure shown in Figure 1. In this process, two or three rows (spaced approximately 1 mm apart) of fourteen microhardness indents each (spaced approximately 0.2 mm apart) were applied along the entire gauge length of each specimen before testing

using a Vickers hardness indenter with an indenting load of 1 kg. In this case, the resulting hemispherical plastic zone is estimated to be less than 30 μm or about 5% of the cladding thickness; subsequent experimental observations showed that the indentations played no significant role in specimen deformation and that the failure path usually ignored the indentations. The distances between the indents were carefully measured for every specimen using a traveling microscope before and after testing, such that the true local strain measured over local elements of 0.20 mm in size with an accuracy of ± 0.01 in strain value.

The ring-stretch tests were performed at both room temperature and 300°C under an initial quasi-static strain rate of 10^{-3}/s. and in a manner that maintained the circular cross-section shape of the cladding. As shown in Figure 2, the tests used a grip arrangement relying on two "D" shaped die inserts and a pin-loaded grip assembly[3]. In order to minimize the friction between the outer surface of the die inserts and the inner surface cladding specimen, the interface was lubricated with two layers of vacuum grease and two layers of Teflon tape at the beginning of each test. In our test procedure, the gauge sections of the cladding test specimens were oriented at the top and bottom of the die inserts, such that a constant specimen curvature was maintained during deformation. As is commonly done in the determination of forming-limit diagrams for sheet metal formability[4], this technique relies on lubrication to minimize the friction coefficient such that load is efficiently transferred to the specimen gauge section.
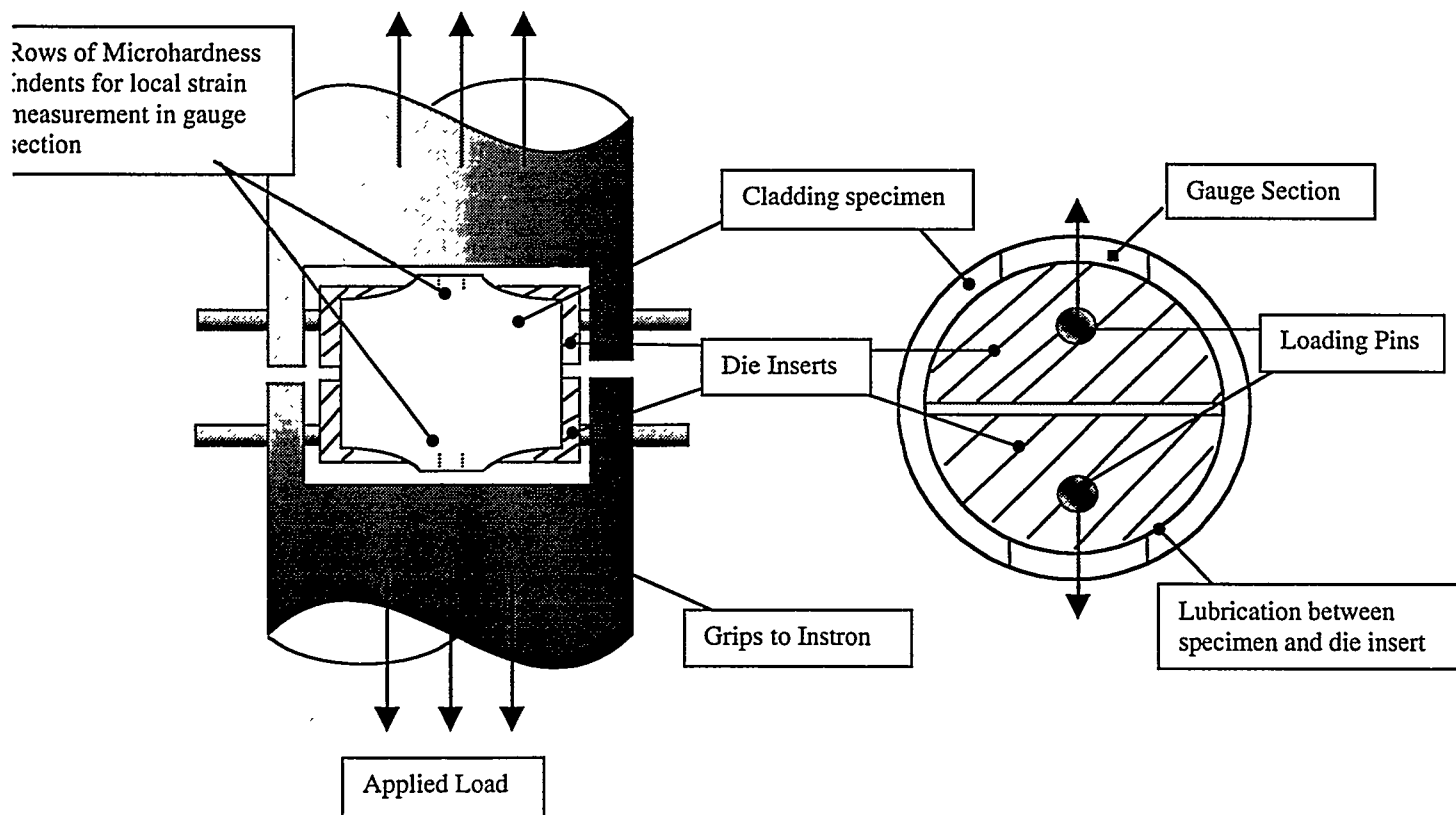

Figure 2. Loading Fixtures for the mechanical tests conducted. The gauge section is oriented on top of the die inserts, and lubrication (Teflon and vacuum grease applied between the specimen and die insert). The spacing between the die inserts and grips is exaggerated for clarity.

Although the fracture strain data were similar in magnitude between the two procedures, there was much larger scatter in fracture-strain values when the gauge sections were located at the die insert openings, possibly because of the bending that these specimens experience when they are tested without a central dogbone insert.

It is also significant that previous researchers concluded that the limit strains at the onset of localized necking (used later in this paper as a failure condition) are independent of interface friction[4]. Finally we recognize that the procedure used here (i.e., specimen gauge sections placed in the top and bottom positions in contact with the dies as in Figure 2) works well for determining *strain* distributions and failure *strains*, but it makes any accurate determination of *stress* very difficult, if at all possible.

RESULTS AND DISCUSSION

Specimen Geometry Effects and Deformation Behavior in Uniaxial Tension

The principal characteristic of the deformation behavior of the Type "C" specimen (gauge length to width ratio of 1:1) is the *absence* of any significant uniform strain at maximum load. This behavior is readily evident in Figure 3, which depicts the strain distributions along the gauge section at both maximum load (the solid lines) and at specimen fracture.
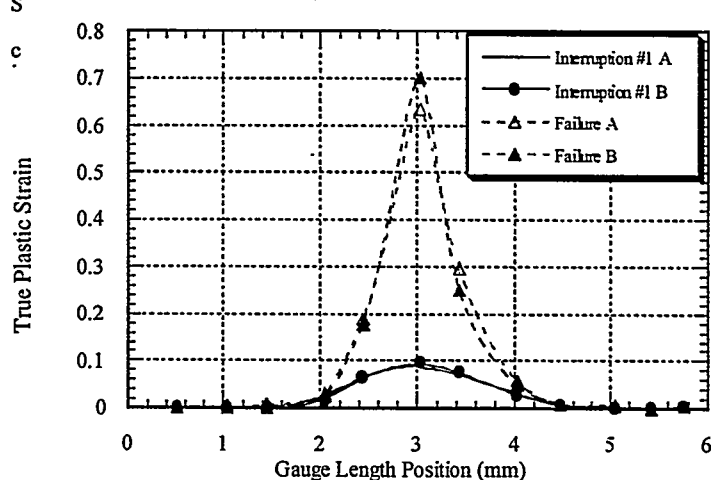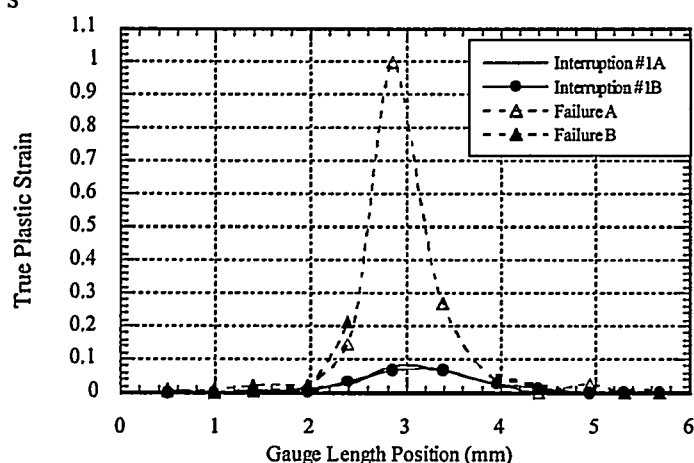

Figure 3: Strain distribution for Type "C" specimen as function of gauge length position for (a) 300 °C and (b) 25 °C quasi-static ring tension

The two lines shown in each figure correspond to strain data obtained from the two rows of microhardness indentations used as grids. These data show that at maximum load, there is already a pronounced strain concentration occurring at the center of the specimen. Thus, specimen deformation at maximum load for this specimen geometry is characterized by a *non-uniform* strain distribution; in fact, very little, if any, uniform strain can be detected. Furthermore, such a non-uniform strain distribution implies specimen necking is already present at maximum load.

Previous tests of transversely oriented compression specimen indicate that the unirradiated Zircaloy-4 cladding material used in this study had a strain hardening exponent ($n = d\ln\sigma/d\ln\varepsilon$) of $n = 0.07$ at room temperature and $n = 0.06$ at $300°C$. It is well known from analysis of tensile tests that diffuse necking should initiate near maximum load at a uniform strain $\varepsilon_u \cong n^{5,6}$. Thus, we should expect uniform strain levels of 0.06-0.07 instead of the observed value of less than 0.02, indicating that "premature" specimen necking has occurred in the Type "C" specimen.
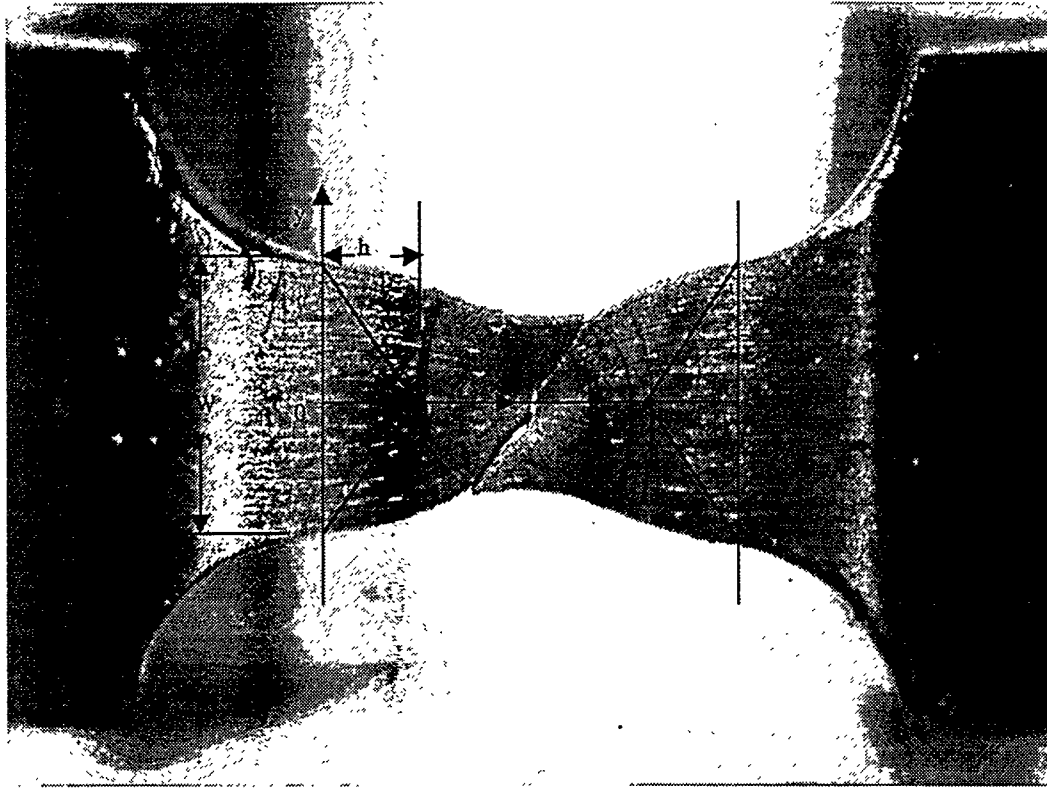
Figure 4: Triangular dead zones formed in type "C" specimen.

The cause of the premature specimen necking behavior is shown in Figures 4 and 5. The strain concentration near the specimen center is quite obvious in the fractured specimen shown in Figure 4. Importantly, also present in Figure 4 are faint surface scratch marks across the gauge length and oriented normal to the tensile axis. These scratch marks were initially straight but became bowed during the test, indicating a displacement gradient *across* the specimen width. Figure 5 shows measurements from three parallel rows of grids along the specimen gauge length, one row being down the middle of gauge section and a row on each side approximately 0.2 mm from the specimen edges. The data in Figure 5 show that the strain gradients across the specimen width not only exist but that the character of the gradient varies with position along the gauge section. Specifically, Figure 5 shows an inversion of strain distributions such that the centerline strains are very large but approach zero a distance h (see Figure 4) from the end of the gauge length. Thus, within a distance h from each fillet, the strain along the specimen centerline is nearly zero despite being finite near the specimen edges. These data as well as careful examination of the deformed specimen surface reveals the presence of two roughly triangularly shaped "dead zones" present near the ends of the gauge section. The cladding material within these dead zones does not deform significantly.

The dead zones in Figure 4 are roughly 1.4 mm high for the Type "C" specimen. Importantly, their presence leaves only a 1.4 mm section along the specimen centerline to deform plastically. Because specimen deformation has to satisfy displacement requirements placed on it by the test fixtures, the effect of the dead zones is to concentrate deformation near the specimen center, as is readily evident in Figures 4 and 5. As a result, while the (extensional) fracture strain is approximately 0.68 at the center of the specimen, it is only about 0.44 near the edges. It is this strain distribution that causes the inversion of the strain gradients along the specimen gauge length such that little or no extensional strain occurs along the centerline within the dead zones, requiring very large extensional strains at the specimen center.
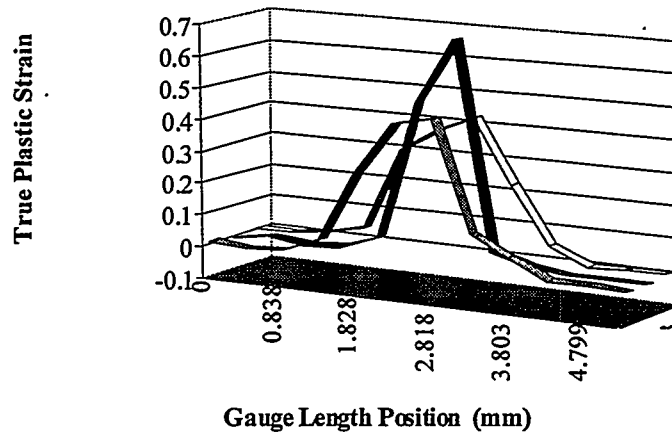
Figure 5: Strain gradient measured across the gauge width for type "C"
specimen tested at room temperature in transverse ring tension.

The inversion of the width-wise strain gradients along the specimen length has the important consequence that specimen necking occurs from the onset of plastic deformation. The presence of the dead zones coupled with the intense strain at the specimen center means that displacements *across* the specimen width are *not* uniform. It is important to note that these width-wise displacements range from small near the fillets at the ends of the gauge length (where the base of the dead zone is largest) to large across the specimen center, where the intense deformation creates large contractions of this plastically anisotropic material across the width. In short, diffuse necking is induced from the onset of fully plastic deformation by the presence of the dead zones and the associated strain gradients. This situation is especially pronounced when the dead zone height is large and for specimens with short gauge length-to-width rations, such as *l/w* ≈ 1. For such a case, a condition of uniform deformation does not exist, and *specimen necking occurs from the onset of fully plastic deformation.* As a result, strains at maximum load are much smaller than expected from geometric necking analyses and do not correlate to a "uniform" strain in the true sense of the term.

On a qualitative basis, we might expect the origin of the dead zones and their height to relate to the plastic anisotropy of the cladding. Specifically, if through-

thickness slip is difficult, we would expect deformation of a tensile specimen to be dominated by slip across the specimen width at an angle such that the intersection of such slip bands might form a dead zone. In fact, previous uniaxial tension measurements (on a different specimen geometry) indicate a plastic anisotropy parameter $R = \varepsilon_{width}/\varepsilon_{thickness} = 2.3$ for the present cladding in the transverse direction of the tube[4]. Such an R value confirms the difficulty of through-thickness slip, or conversely the ease of slip across the width of a tensile specimen. Given the grip constraints, such slip will tend to occur on planes of high shear stress inclined across the specimen width. Slip across the specimen width on two such intersecting slip "systems" would create a deformation near the ends of the gauge section characterized by triangular shaped dead-zone regions.

As shown in Figure 6, finite-element analysis (FEA) of the Type "C" specimen confirms the presence of large plastic strain gradients in the width as well as the axial directions. It also confirms the inversion of the width-wise strain gradient along the specimen length. Consistent with experimental observations such as Figures 4 and 5, the FEA results also confirm the presence of a "dead zone" at the ends of the gauge length. Importantly, such behavior is coupled with intense deformation near the apex of the dead zone; it is this combination that drives the

necking behavior so pronounced in the short Type "C" specimen. From the standpoint of obtaining meaningful constitutive stress-strain data, the necking behavior described above makes the Type "C" specimen unacceptable.

Finite element analyses indicate that the inherent incompatibility in the transverse plastic deformations of the gauge section and shoulder regions of the uniaxial specimen results in the strain concentrations near the outer edges of the gauge length at fillet junction, the magnitudes of which depend on the specimen geometry. These strain concentration effects are damped out with increasing distance from the fillet junction. The damping of the stress concentrations along the specimen length suggests a minimum gauge length is needed before the stress-strain distributions at the center tend toward being relatively homogenous. Consistent with the discussion above, the minimum gauge length is considerably longer for an anisotropic material like unirradiated Zircaloy, where texture inhibits through-thickness slip, than for normal plastically isotropic materials. If the gauge length of the uniaxial Zircaloy specimen is too short (e.g., $l/w = 1$), the FEA confirms the plastic strain distribution in the entire gauge length is non-uniform from the onset of yielding.

As shown in Fig. 6 analysis indicates that a significant fraction of the gauge length of the Type "D" specimen with $l/w = 4$ deforms homogeneously (the analyses assumed the presence of a central dogbone insert to prevent bending). Note that the strain concentration effect, discussed earlier, occurs both in a ring stretch (curved) specimen as well as in a flat specimen with the same geometry, and is not a consequence of the curved geometry of the ring stretch specimen.. Consistent with the analysis, tensile tests of Type "D" specimens with $l/w = 4$ (see Figure 1) confirm a greater extent of uniform deformation as well as strain values at maximum load ($\varepsilon \cong 0.04$) that approached (but did not equal) the values expected from the mechanics of diffuse necking in uniaxial tension ($\varepsilon = n \cong 0.07$). Significantly, experiments show that in these cases specimen necking occurs at the ends of the gauge

A   = .003783
B   = .011349
C   = .018914
D   = .02648
E   = .034046
F   = .041612
G   = .049177
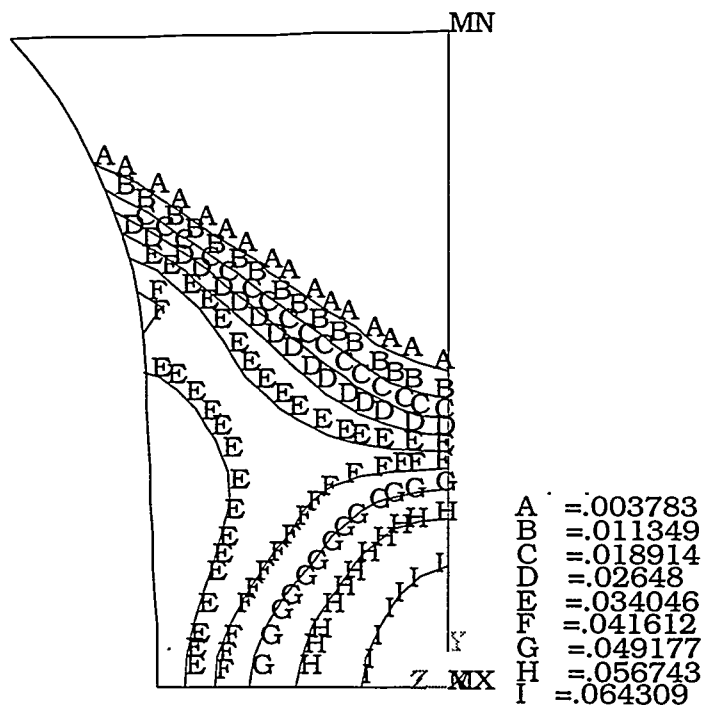H   = .056743
I   = .064309

Fig. 6   Contour plot of axial (ring hoop) plastic strain in the anisotropic ring stretch specimen type "C" at the outer diameter surface. The large plastic strain gradients in the axial and width directions make this specimen design unacceptable.
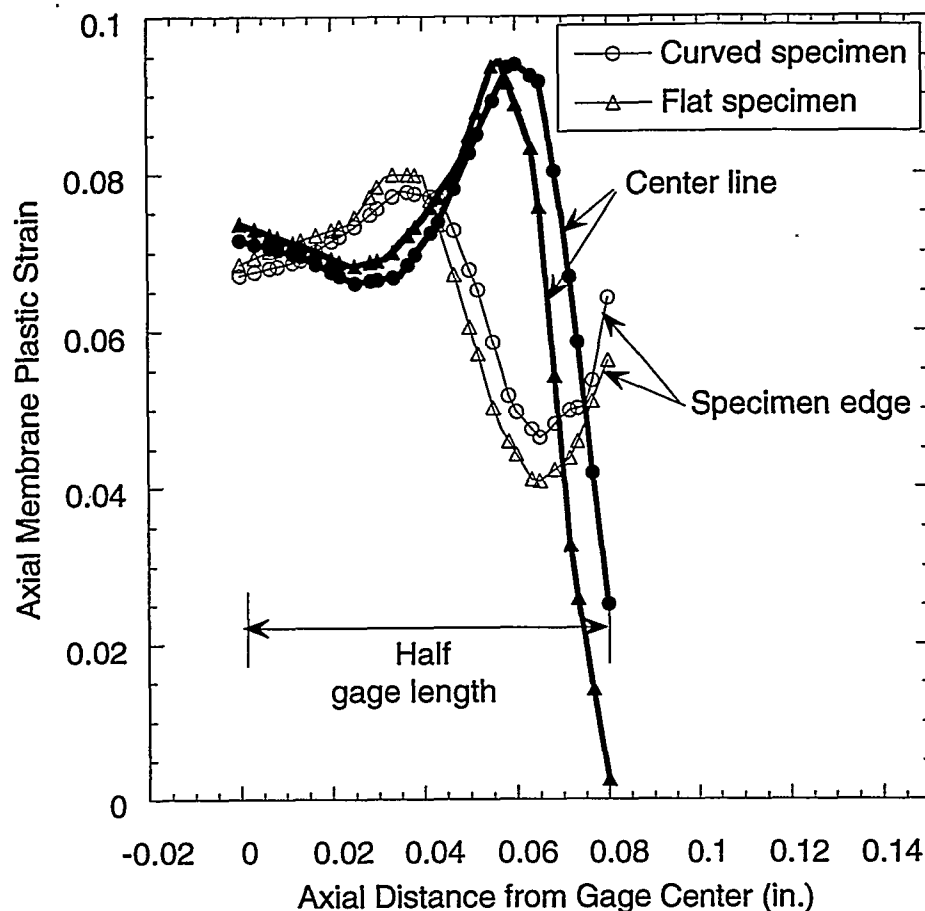
Fig. 7. Comparison of axial membrane plastic strain distributions along the centerline and along the specimen edge of a curved specimen (type "D") and a flat specimen ($l/w=4$).

section (near the strain peaks in Fig. 7), suggesting continued effects of strain gradients present at the junction of the fillets and gauge section. It should be noted that although the uniform elongation can be significantly underestimated in Type "D" specimens, the ultimate tensile strength is not, because of the low strain hardening in Zircaloy.

In summary, the combination of the plastic anisotropy of the Zircaloy cladding (i.e., difficult through-thickness slip) and a short gauge length (l/w =1) results in tensile behavior characterized by necking from the onset of yielding. For at least the plastically anisotropic case, valid measures of the constitutive stress-strain response of Zircaloy cladding should rely on tensile specimens with gauge length-to-width ratios of at least 4 to minimize

the specimen geometry effects that induce premature specimen necking. Such tests will also require care in minimizing any friction effects that might also assist specimen necking.

Failure Behavior in Uniaxial and Plane-Strain Tension : As is evident from the path of fracture shown in Figure 4, failure of the Zircaloy cladding tube under the uniaxial ring-stretch condition occurs on a plane inclined across the specimen width as a result of the deformation localization process. Ductility data from these specimens are clearly affected by the specimen geometry and the resulting necking process, and such data are not likely to be representative of a material deforming uniformly in

uniaxial tension. Furthermore, while the uniaxial ring tests fail on a plane inclined across the width of the specimen, *ductile* failure of cladding tubes by hoop expansion occurs predominantly due to through-thickness slip with a failure path inclined through the cladding thickness. Thus, the failures of the uniaxial specimens and cladding tubes under hoop expansion involve two different modes of slip. In addition, in-service failure of the cladding tubes is likely to occur under biaxial states of stress. As a result, failure ductility data from uniaxial tension tests are not likely to be an accurate indicator of cladding failure.

The requirement that cladding failure occur by hoop expansion due to through-thickness slip under some degree of biaxial tension suggests the use of a plane-strain ring-stretch test. Based on experimental analysis and finite element analysis, assuming a plastically isotropic material, we previously developed a "double edge-notched" plane-strain test geometry for use in a ring-stretch test[4]. In the present study, we have used a plastically anisotropic finite element analysis to further evaluate the deformation response of the double edge-notched plane-strain ring specimen. These results show that significant plastic deformation of the specimen is needed before about half the width of the minimum cross section is under a sufficiently biaxial state of stress in order to deform in an approximately plane-strain manner. Once plane-strain deformation is attained, the axial stress distribution becomes relatively uniform, and the plane-strain axial flow stress can be related to the measured load. Owing to the lack of a well-defined gauge length, the average axial plastic strain in this specimen cannot be directly related to the measured displacement. Thus, ductility data have to be obtained experimentally. Furthermore, the ductility data obtained in the plane strain test will be a valid measure of plane-strain ductility provided failure initiates near the center of the gauge length (where near plane-strain deformation exists) and propagates towards the edge, rather than initiating at the notch edges and propagating inward. Experiments using plane-strain ring stretch tests of unirradiated Zircaloy-4 specimens confirm that failure initiates near the specimen centerline, as expected.

SUMMARY

In summary, our results indicate the importance of specimen design in selecting a ring specimen geometry that will yield meaningful mechanical properties and ductility data and reproduce the loading conditions present during an RIA. Our experiments and analysis show that for Zircaloy tubing, data such as uniaxial yield strengths and stress-strain curves are better achieved by using a uniaxial specimen whereas ductility data that are applicable to RIA transients are better achieved using a plane-strain specimen. If significant plastic anisotropy exits, uniaxial ring tests should be performed on specimens with gauge length to width ratios of at least 4. However, the tubing geometry does not allow for very large l/w values, and thus uniaxial ring specimens may be inherently susceptible to the types of limitations observed in the present tests. Given that failure can be induced on through-thickness planes in plane-strain specimens, ductility values derived from this geometry are likely more applicable for predictions of thermally-induced RIA-like cladding failures.

ACKNOWLEDGMENTS

REFERENCES

1. Meyer, R. O., McCardell, R. K., Chung, H. M., Diamond, D. J., and Scott, H. H., , "A Regulatory Assessment of Test data for Reactivity Initiated Accidents," *Nuclear Safety*, 37(4), (1996) 872-387.
2. Mahmood, S. T., and Murty, K. L., "Effect of Tensile Deformation on Crystallographic Texture in Zircaloy Sheet", *9th International Symposium on Zr in the Nuclear Industry*, Kobe, Japan, ASTM STP 1132, (1991) 119-139.
3. Hecker, S. S., *Sheet Metal Industries*, 52, (1975), 671-676.
4. Link, T.M., Koss, D.A., and Motta, A.T., "Failure of Zircaloy cladding under transverse plane strain deformation", Nuclear Engineering and Design 186 (1998) 379-394.
5. Considère, A., *Ann. Ponts et Chaussées*, vol. 9, (1885), 574-775.
6. Hart, E.W. *Acta Metallurgica*, vol. 15, (1967), 351-355.